Journal of Alloys and Compounds 935 (2023) 168117

Contents lists available at ScienceDirect

Journal of Alloys and Compounds

journal homepage: www.elsevier.com/locate/jalcom

Structural features of $Cu_2Mg_xZn_{1-x}SnS_4$ solid solution films for third-generation solar cells

Maksym Yermakov [a,*], Roman Pshenychnyi [a], Anatoliy Opanasyuk [a], Yuriy Gnatenko [b], Oleksii Klymov [c], María del Carmen Martínez-Tomás [c], Vicente Muñoz-Sanjosé [c]

[a] Sumy State University, Rimsky-Korsakov str., 2, Sumy UA-40007, Ukraine
[b] Institute of Physics of National Academy of Sciences of Ukraine, 03028 Kyiv, Ukraine
[c] Universitat de València, C/Dr. Moliner 50, 46100 Burjassot, Spain

ARTICLE INFO

Article history:
Received 21 June 2022
Received in revised form 11 November 2022
Accepted 15 November 2022
Available online 17 November 2022

Keywords:
$Cu_2Mg_xZn_{1-x}SnS_4$
Semiconductor
Chemical synthesis
Spray pyrolysis
X-ray diffraction
Raman spectroscopy

ABSTRACT

The paper studies the influence of the ratio of Mg/Zn molar concentrations in the precursor ($0 \le y \le 0.5$) on the structural, substructural, optical characteristics and chemical composition of $Cu_2Mg_xZn_{1-x}SnS_4$ films deposited by the spray pyrolysis method from molecular solutions. The data of X-ray structural studies indicate the formation of single-phase films with the structure of kesterite. The single-phase structure is also confirmed by studies of Raman spectra for samples obtained at $y \le 0.3$. Chemical analysis of the films confirms the successful inclusion of Mg in thin layers up to the level of (5.5–6.7) at%. An increase in the total amount of Mg has little effect on the concentration of all elements except zinc. The introduction of magnesium changes the lattice constants of the material, the sizes of coherent scattering regions, the level of microdeformations, and the density of dislocations in the films. At the same time, the layers obtained at $y = 0.1$ have the minimum total concentration of dislocations ($0.73 \cdot 10^{17}$ lin/m^{-2}). Thus, replacing zinc with magnesium increases the quality of the solid solution at concentrations $y < 0.3$. The band gap of the undoped Mg compound was found to be 1.47 eV, and for the Mg-doped samples it decreases from 1.28 eV ($y = 0.1$) to 1.22 eV ($y = 0.5$). Thus, based on the obtained results, the $Cu_2Mg_xZn_{1-x}SnS_4$ solid solution can be considered as an inexpensive material for creating absorption layers of thin-film solar cells.

1. Introduction

Finding environmentally friendly energy sources is one of the most important tasks of our time. One of the most promising of these sources is the energy of solar radiation. The best way to convert solar energy into electricity is photovoltaic conversion.

Amongst other materials and approaches, Cu_2ZnSnS_4, $Cu_2ZnSnSe_4$, and $Cu_2ZnSn(S_xSe_{1-x})_4$ compounds with a kesterite structure have been proposed as absorbing layers of third-generation film solar cells (SCs) [1–3]. An advantage of these materials over others is the absence of environmentally hazardous and rare components. On the contrary, the elements that are part of them are widespread in the earth's crust, and the cost of their extraction is relatively low. However, at present, photovoltaic devices created using $Cu_2ZnSn(S_xSe_{1-x})_4$ absorption layers have achieved efficiencies of only 11.3% [4].

One of the reasons for the low effectiveness of SCs based on kesterite compounds is their narrow range of homogeneity and multi-component nature. Therefore, it leads to the formation of a large number of secondary phases (CuS, Cu_2S, ZnS, SnS, SnS_2 and Cu_2SnS_3 for Cu_2ZnSnS_4) and their structural defects (vacancies V_{Cu}, V_{Zn}, V_{Sn}, V_S, V_{Se}, interstitial atoms Cu_i, Zn_i, Sn_i,S, antistructural defects Cu_{Zn}, Zn_{Cu}, Zn_{Sn}, Sn_{Zn}, as well as defective complexes $V_{Cu} + Zn_{Cu}$, $2Cu_{Zn} + Sn_{Zn}$, $Zn_{Sn} + 2Zn_{Cu}$) when the stoichiometric composition of the compound is disturbed [5].

Another reason for the low efficiency of photoconverters is that these devices inherited their design from the previous generation of SCs based on $CuIn_{1-y}Ga_ySe_2$ (CIGS) compounds [6]. As a result, they have suboptimal coordination of energy zones and lattice periods of contact materials. However, the main limitation of the efficiency of photoconverters based on kesterite compounds is due to their low no-load voltage (V_{oc}) compared to the width of the bandgap [7]. Several authors found that, in this case, defects are the main factor

* Correspondence to: Rimsky-Korsakov str., 2, Sumy UA-40007, Ukraine.
E-mail addresses: m.yermakov@ekt.sumdu.edu.ua (M. Yermakov), pshenychnyi@gmail.com (R. Pshenychnyi), a.opanasyuk@ekt.sumdu.edu.ua (A. Opanasyuk), yuriygnatenko@ukr.net (Y. Gnatenko), oleksii.klymov@uv.es (O. Klymov), carmen.martinez-tomas@uv.es (M. del Carmen Martínez-Tomás), Vicente.Munoz@uv.es (V. Muñoz-Sanjosé).

https://doi.org/10.1016/j.jallcom.2022.168117

that creates deep levels in the band gap and forms the tails of energy states for the allowed energy bands [8,9].

In earlier works [10,11], the defects associated with Cu-Zn disorder were considered to be the main reason for the large V_{oc} deficit. It was believed that the low energy of formation of such defects as Cu_{Zn} and Zn_{Cu}, due to the proximity of chemical properties and radii of Zn and Cu atoms, leads to a high concentration of anti-structural defects Cu / Zn in Cu_2ZnSnS_4. Therefore, some approaches have been proposed to reduce the probability of such disorder, for example, partial substitution of Cu^+ ions by Ag^+[12], Zn by Cd, Mn, or Ba [13,14]. In many works, a positive effect of cationic substitution on the improvement of photoelectric characteristics of SCs was demonstrated.

Recently, it was recognized that other point defects, namely Sn_{Zn}, have the greatest effect on the decreased V_{oc} SCs based on the compound Cu_2ZnSnS_4 [15,16]. Later, it was found that these anti-structural defects not only affect the deep donor states in the band gap of the material but also form defective complexes with Cu_{Zn} defects, which have a high concentration. Defective complexes [$2Cu_{Zn}$ + Sn_{Zn}] are considered the main reason for the formation of energy states in the tail, which reduce the band gap of Cu_2ZnSnS_4. Therefore, it was proposed to suppress the formation of anti-structural defects Sn_{Zn} by replacing Sn with an element of the same group of the table of elements – Ge [17,18].

Another way to solve this problem is to replace zinc with elements such as Fe, Mn, and Cd with the formation of Cu_2FeSnS_4, Cu_2MnSnS_4, and Cu_2CdSnS_4 films [19–21], or even replacing two elements Cu and Zn with the formation of compounds Ag_2MnSnS_4, $Ag_2ZnGeS(Se)_4$ [22–24]. Because some of these elements are toxic or can cause undesirable effects of magnetism in photovoltaic devices, a solid solution of $Cu_2Mg_xZn_{1-x}SnS_4$ has been proposed as a promising candidate for absorbing layers of thin-film heterojunction SCs [25]. Besides, recent theoretical and experimental works [26–28] have shown that the solid solution of $Cu_2Mg_xZn_{1-x}SnS_4$ can be a thermodynamically stable material suitable for photovoltaic applications.

It should be noted that adjusting the band gap of Cu_2ZnSnS_4 by replacing Zn with Mg is more advantageous compared to other elements. First, in contrast to Na, K, and Sb ions, Mg^{2+} ions occupy Zn^{2+} places in the lattice and do not segregate on the surface and/or grain boundaries because the radii of Mg^{2+} and Zn^{2+} are very similar. In addition, the introduction of Mg into the Cu_2ZnSnS_4 layer has unique advantages over other impurities due to its low cost, high reserves in the earth's crust, and the environmental friendliness of this element. Magnesium is more common than Zn, cheaper than Ge, and more environmentally friendly than Cd and Se. Finally, the introduction of Mg can eliminate or reduce the formation of some possible Cu_2ZnSnS_4 secondary phases. For example, the binary phase of ZnS, which is often formed in the synthesis of a kesterite compound, is stable, but the MgS phase is unstable [29]. These advantages make the substitution of Zn by Mg a productive approach to regulating the band gap of Cu_2ZnSnS_4.

In our previous works, the synthesis of nanoparticles (NPs) of Cu_2ZnSnS_4 and $Cu_2ZnSnSe_4$ compounds were optimized using different sources of chalcogen in the precursor [30]. Cu_2ZnSnS_4 films were obtained by spraying inks based on their suspensions [31]. The structural characteristics and chemical composition of Cu_2ZnSnS_4 films during low-temperature annealing in argon were investigated. Subsequently, a method for the synthesis of $Cu_2ZnSn(S_xSe_{1-x})_4$ solid solution NPs was developed. This method makes it possible to obtain an almost single-phase semiconductor material with a controlled composition from x = 0 to x = 1. As a result, inks based on $Cu_2ZnSn(S_xSe_{1-x})_4$ solid solutions were developed [32].

The aim of the presented work was to determine the effect of doping the compound Cu_2ZnSnS_4 with magnesium on the chemical composition and some structural and optical characteristics of the films obtained by spraying molecular solutions in a wide range of changes in the concentration of magnesium in the precursor, namely y = (0 – 0.5). For this purpose, we studied the effect of the Mg content in the precursor on the phase and chemical composition, surface morphology, texture quality, lattice constants, the size of the coherent scattering regions, microdeformations, and the optical density of the films. Based on the research results, a conclusion was made about the optimal characteristics of $Cu_2Mg_xZn_{1-x}SnS_4$ films for use as SCs absorbing layers.

2. Materials and methods

The following aqueous solutions were used as precursors $Cu_2Mg_xZn_{1-x}SnS_4$: $Zn(CH_3COO)_2$, $CuCl_2$, $SnCl_2$, $MgCl_2$, and $(NH_2)_2CS$ with a molar concentration of 0.5 mol/l. The following chemical reagents were used to create them: $Zn(CH_3COO)_2{\cdot}2\ H_2O$ (for analysis EMSURE ACS, ≥99.5%, Supelco), $CuCl_2{\cdot}2\ H_2O$(ACS reagent, ≥99.0%, Sigma-Aldrich), $SnCl_2{\cdot}2\ H_2O$ (ACS reagent, ≥98.0%, Sigma-Aldrich), $MgCl_2{\cdot}6\ H_2O$ (ACS reagent, ≥99.0%, Sigma-Aldrich), and $(NH_2)_2CS$ (ACS reagent, ≥99.0%, Sigma-Aldrich). To obtain a $SnCl_2$ solution, a small amount of concentrated hydrochloric acid was added to prevent hydrolysis. In the next step, the resulting solutions were mixed. A magnetic stirrer with a Teflon rod and a 50 ml glass beaker was used for this purpose. Solutions of salts in stoichiometric amounts of Cu: Zn(Mg): Sn: S = 2: 1: 1: 4 were gradually added to the thiourea solution using graduated pipettes. The ratio between the concentrations of zinc and magnesium y was taken as 0.9:0.1; 0.8:0.2; 0.7:0.3; 0.6:0.4 and 0.5:0.5. As a result, transparent molecular solutions with different ratios of concentrations of Zn: Mg atoms were obtained.

In order to obtain the films, the obtained molecular solutions were sprayed on glass substrates, which were cleaned using a UV Ozone Cleaner. Spraying of molecular solutions was performed using an airbrush with a nozzle diameter of 0.3 mm at an operating pressure of 0.2 MPa. The distance between the airbrush and the substrate was 20 cm. Argon was used as the carrier gas. Glass substrates were placed on a heated plate that maintained a temperature of 350 ºC. To form the film, the spraying procedure was performed cyclically. The number of spray cycles performed for film application was 100. The duration of one cycle was 6 s, where 2 s was the duration of the spray and 4 s was the pause. Fig. 1 shows the method of synthesis of molecular solutions and the application of films.

The morphological properties of the synthesized films were investigated using a Hitachi S-4800 scanning electron microscope, which is equipped with a Bruker X-ray detector for microanalysis of samples. The voltage in the microscope pillar was ~ 20 kV, and the approximate working distance to obtain images with good resolution - was 8 mm. Magnification of the image was carried out in the range from 250 to 150000. The thickness of the samples was determined by photographing the chipped films.

An AZtecOne energy-dispersive spectrometer with X-MaxN20 detector (manufactured by Oxford Instruments plc) of the SEO-SEM Inspect S50-B scanning electron microscope and a Bruker microscope microanalyzer were used to study the chemical composition of the obtained samples. Chemical analysis of the material was performed at least three points on the surface of the sample, after which the measurement results were averaged.

Ni-filtered K_α radiation of the copper anode of the X-ray diffractometer DRON 4–07 with the established mode of operation of the X-ray tube was used to study the structural characteristics of the samples: U = 30 kV; I = 20 mA. The range of 2θ-θ diffractograms was 20–80°, where θ is the Bragg angle. X-ray focusing was performed by the Bragg-Brentano method. The obtained diffractograms were normalized to the peak intensity (112) of the tetragonal phase of the compound. In the phase analysis, a comparison of the relative

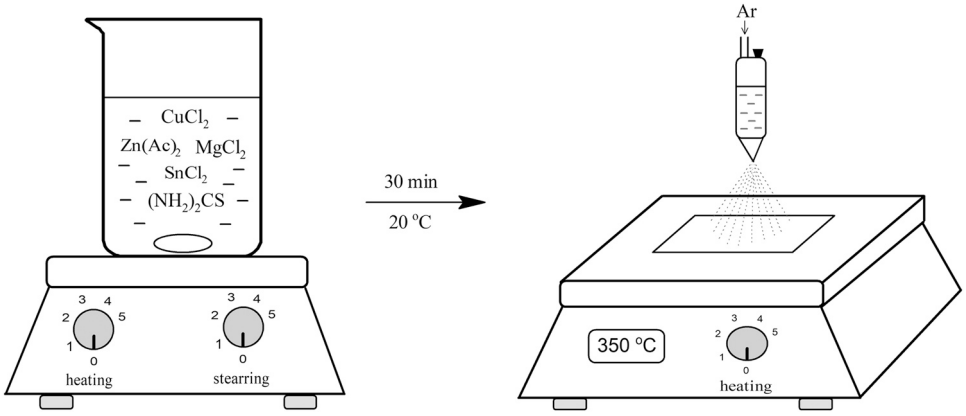

Fig. 1. The method of obtaining molecular solutions and the scheme of depositing $Cu_2Mg_xZn_{1-x}SnS_4$ films by the spray technique.

intensity and interplanar distances of the studied samples and the standard sample was performed (JCPDS № 01–075–4122).

The texture of the films was evaluated according to the Harris method [33]. The polar density was calculated using the expression:

$$C_i = (I_i/I_{0i})/(1/N\sum_{i=1}^{N}(I_i/I_{0i})), \quad (1)$$

where I_i, I_{0i} – the integral intensities of the i-th diffraction peak for the film sample and reference; N – the number of lines present on the radiograph. Reference data were taken from JCPDS crystallographic cards.

Next, the dependences of C_i – $(hkl)_i$ and C_i - φ were constructed. Where φ – the angle between the axis of the texture and the perpendicular to different crystallographic planes (to which the reflections on the diffractograms correspond); (hkl) – Miller indices. The texture axis has the indices corresponding to the largest value of C_i. The orientation factor f in each direction can be calculated from the expression $f = (1/N\sum_{i=1}^{N}(C_i - 1)^2)^{1/2}$.

The calculation of the lattice constants a, c for the tetragonal phase of the solid solution $Cu_2Mg_xZn_{1-x}SnS_4$ was carried out by reflections from the crystallographic planes (112), (220), and (116) using the following relations [34]:

$$a=\lambda/(2\sin\theta)(h^2+k^2+l^2(a/c)^2)^{1/2}, \quad (2)$$

$$c=l/(-(h^2+k^2)/a^2+(2\sin\theta/\lambda)^2)^{1/2}, \quad (3)$$

where λ – the length of X-rays; h, k, l – Miller indices; θ – Bragg angle.

The Nelson-Riley extrapolation method was used to calculate the precise values of the lattice constants [35]. For this, the extrapolation function $a(c) - 1/2\cos^2\theta(1/\sin(\theta) + 1/\theta)$was selected. Linear approximation of the obtained points was carried out using the method of least squares.

The unit volume of materials was calculated using formula:

$$V_{unit}=a^2c. \quad (4)$$

The X-ray diffractometric method was also used by us to determine the average size of the coherent scattering regions (CSR) L and the level of microdeformations ε in the films of the studied material along the full width at half maximum (FWHM) of the diffraction lines. The size of the CSR (L) and the level of microdeformations (ε) in the obtained samples were calculated by the physical broadening of the most intense diffraction peaks according to the formulas [36]:

$$L=0.94\lambda/(\beta\cos\theta), \quad (5)$$

$$\varepsilon=\beta\cos\theta/4, \quad (6)$$

where β – the value of the width of the corresponding diffraction peak.

It is known that the average density of dislocations in films, which are effective recombination centers in semiconductor materials, can be estimated by the magnitude of microdeformations (ε) and the size of the CSR (L). Accordingly, their concentration in the material should be minimized.

The sample-averaged density of dislocations forming block boundaries, according to [37], is equal to:

$$\rho_L=3\,n/L^2, \quad (7)$$

where n – the number of dislocations on each of the six faces of the block.

If the dislocations are located mainly in the middle of the CSR, the density of dislocations can be calculated from the expression [37]:

$$\rho_\varepsilon=4/F\cdot(2\varepsilon/d_0)^2, \quad (8)$$

where F – a number that takes into account how many times the energy of a dislocation increases when it interacts with other dislocations; d_0 – the lattice period in the corresponding direction.

Taking $n = F = 1$ according to relations (7), and (8), it is possible to estimate the lower limit of ρ_L and the upper limit of ρ_ε.

A slightly different expression for estimating the total density of dislocations in the material is given in [38]:

$$\rho_{\varepsilon L}=15\varepsilon/(d_0L). \quad (9)$$

Thus, relations (7–9) make it possible to estimate the concentration of dislocations that are in the volume of the CSR, at their boundaries, and the total concentration.

All procedures for processing the profile of diffraction lines: background extraction, smoothing, separation of K_α doublet - were performed using traditional diffractometer software, namely - the DIFWIN software package.

The Renishaw InVia 90V727 spectrometer was used to study Raman spectra of the obtained films. The measuring range was set within the frequencies (100–800) cm^{-1}. Measurements were performed at room temperature. Lasers with radiation wavelengths $\lambda = 532$ nm and $\lambda = 785$ nm were used as sources of radiation. The spectrum of each sample was measured several times with a time delay of about 5 s. The calibration of the measuring device was performed according to the position of the oscillation mode 520 cm^{-1} from the silicon crystal.

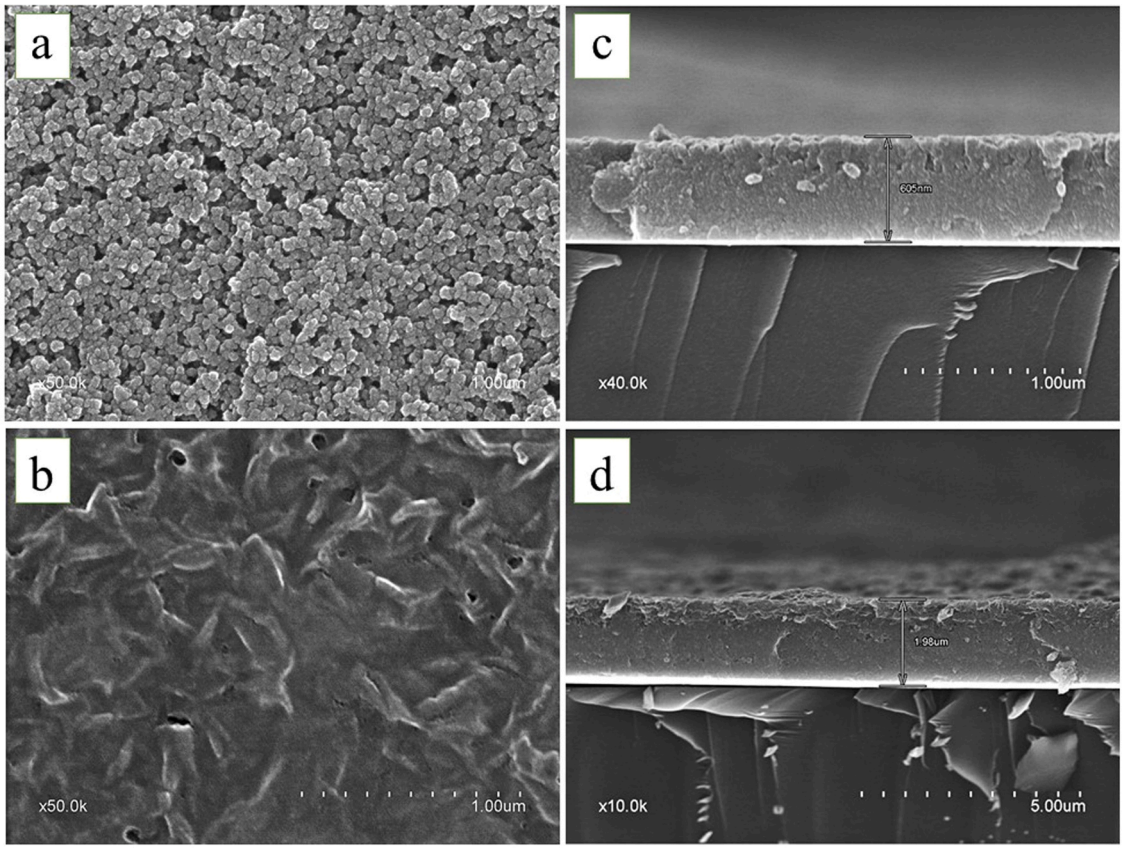

Fig. 2. Electron microscopy images of the surface of $Cu_2Mg_xZn_{1-x}SnS_4$ films (a, b) obtained from precursors containing a nominal Mg value of $y = 0$ and 0.2 respectively, and their cross-sections (c, d).

An SDL-1 grating spectrometer was used to study the absorption spectra. In this case these spectra was excited by an incandescent lamp. We also used a USB spectrometer MAYA 2000-pro (Ocean Optics) to study the photoluminescence (PL) spectra which were excited by an LED with $\lambda = 385$ nm and $P = 100$ mW. Optical measurements were carried out at room temperature. Luminescence was recorded at a temperature of $T = -196$ ºC Experimental methods used in this work are discussed in more detail in [39,40].

3. Results and discussions

Typical electron microscopic images of the surface of the deposited layers of $Cu_2Mg_xZn_{1-x}SnS_4$ and their cross-sections are presented in Fig. 2. Micrographs of the surface of the films show that these layers are quite homogeneous in surface and have a polycrystalline structure. The film thickness was (0.6–5.1) μm and increased with increasing magnesium content in the precursor.

Using the method of X-ray diffraction analysis, we studied the phase composition of $Cu_2Mg_xZn_{1-x}SnS_4$ films and evaluated the quality of their crystal structure. Diffractograms obtained from layers of solid solutions with different contents of magnesium and zinc atoms are shown in Fig. 3 a. As can be seen from the figure, there are peaks at the positions (28.35–28.50)º, (47.15–47.55)º, and (55,95–56,10)º. In some cases, weak peaks were also found at the positions (32.94–32.99)º.

Comparison of the obtained results with the standard shows that they correspond to reflections from the crystallographic planes (112), (220), (116), and sometimes (200) of the kesterite phase of the Cu_2ZnSnS_4 compound (JCPDS card № 01–075–4122). No reflections from the secondary phases were detected on the recorded diffractograms. This indicates that the introduction of magnesium does not change the type of crystal lattice of the compound Cu_2ZnSnS_4.

It was established that films obtained from solutions containing a small amount of magnesium ($y \le 0.2$) had a growth texture [200] (Fig. 3b). When the content of impurities in the precursor increased, the quality of the texture parameter improved. With a further increase in the concentration of Mg ($0.3 < y \le 0.4$), the texture axis changed to [116], with a significant deterioration of its quality. Finally, the films obtained from the precursor with the concentration of magnesium equal to $y = 0.5$ had a texture [220]. Compared with the layers deposited from the precursor with $y = 0.4$, the quality of the texture parameter of the sample with the doping admixture $y = 0.5$ slightly improved.

It is well known that the introduction of impurities of different radii into the Cu_2ZnSnS_4 compound compared to the initial composition usually leads to changes in the lattice parameters of the material and, accordingly, the shift of the diffraction peaks on the diffractograms[41,42]. To study these processes, we determined the period of the crystal lattice of the solid solution. Reflections from the crystallographic planes (220), and (116) were used to calculate the lattice constants. It should be noted that since the studied films were nanostructured and the width of the diffraction peaks was large, in some cases there was an overlap of the diffraction peaks (112), (103) and (200). This led to a shift in the real position of the peak (112) and errors in determining the lattice period. Therefore, such peaks were not used for calculations. Using only the diffraction peak (220), it was possible to determine the lattice parameter a, since the Miller index l for it is zero. That is why table 1 shows the data for the determination of the lattice constants a, c of the material only by the position of reflection from the crystallographic plane (116) and a by the position of the peak (220). The Nelson-Riley extrapolation method was additionally used to determine the lattice constants of the material. These results are also presented in Table 1 ($a_{N\text{-}R}$, $c_{N\text{-}R}$).

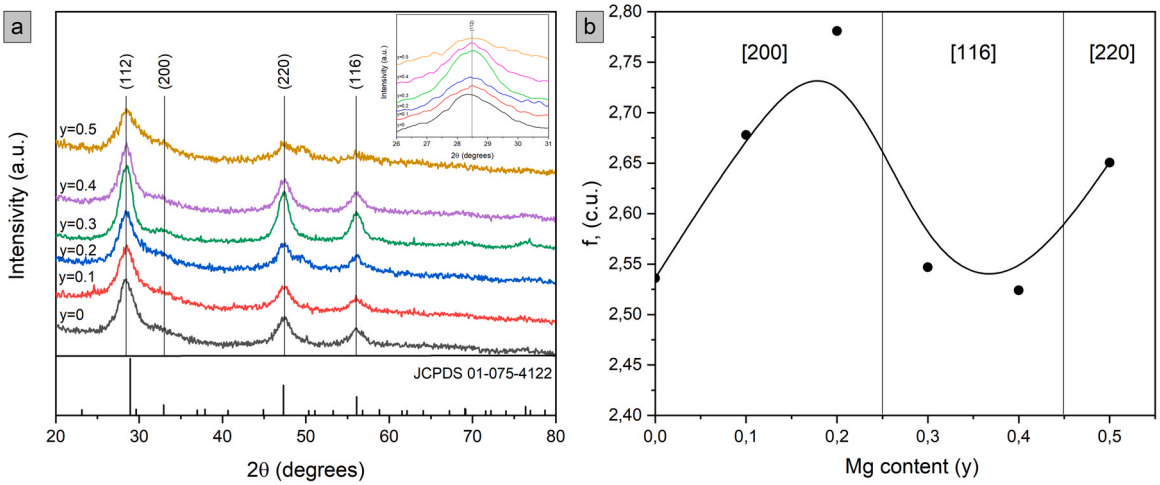

Fig. 3. Diffractograms of films $Cu_2Mg_xZn_{1-x}SnS_4$ obtained from precursors with different magnesium content; the inset shows an enlarged view of the diffraction peak (112) (a). Dependence of the orientation factor on the magnesium content in the precursor (b).

We also calculated the ratio $c/2a$ and the volume of the unit cell of the solid solution V_{unit}.

As can be seen from Table 1, the lattice constants of solid solution films initially decrease slightly with increasing magnesium content in the precursor and then grow. The minimum values of the a - parameter ($a_{N\text{-}R}$ = 0.54099 nm, $a_{(220)}$ = 0.54043 nm) are observed for the layer obtained from the solution corresponding to the magnesium content $y = 0.1$. With a further increase in magnesium concentration, these values increase monotonically. The parameter a found from reflections (116) behaves similarly, but its minimum value ($a_{(116)}$ = 0.54265 nm) is observed at the concentration of magnesium in the precursor $y = 0.2$. At the same time, the values of the lattice constant a found by the position of the peak (220) turned out to be smaller than those found by other methods. When determining the crystal lattice parameter c using the Nelson-Riley method, its constant increase is observed with increasing in the magnesium content in the precursor. At the same time, the $c_{(116)}$ - y curve has a minimum at $y = 0.2$ ($c_{(116)}$ = 1.08468 nm). It should be noted that the values of a, c given in the table are close to the reference results presented in the papers [43,44].

The replacement of Zn^{2+} ions by Mg^{2+} ions in the sites of the crystal lattice of the $Cu_2Mg_xZn_{1-x}SnS_4$ compound should lead to some increase in the lattice constants of the solid solution since the covalent radius of Mg^{2+} (0.136 nm) is greater than that of Zn^{2+} (0.125 nm). However, in some works an increase in the lattice periods of the material (shift of diffraction peaks) is reported [27,42] while in others a decrease [45] is shown. In some papers, the lattice periods of the material did not change [46,47]. Thus, the increase in lattice constants is associated with the replacement of zinc atoms with magnesium atoms in the sites of the crystal lattice. At the same time, the process of reducing the lattice period of solid solution films with a low magnesium content ($y = 0.1$–0.2) is not completely clear. It is shown that in the samples, the dependence of the unit cell volume on the magnesium content in the precursor is similar to the dependencies of $c_{(116)} - y$ and $c_{N\text{-}R} - y$.

Features of the substructure of $Cu_2Mg_xZn_{1-x}SnS_4$ films can significantly affect the functional characteristics of devices based on them. It is known that dislocations that form low-angle boundaries of CSR and lead to microdeformation in films can act as traps or deep recombination centers for charge carriers, determining the electrophysical characteristics of the material, including the life of charge carriers[48]. This determines the relevance of the study of substructural characteristics of films of solid solutions depending on the conditions of their synthesis and magnesium content, in order to optimize them, i.e. the determination of technological parameters at which the concentration of these defects is minimal.

We used the X-ray method to determine the size of the CSR L and the level of microdeformations ε in the studied films. The calculation of these values was performed by reflections from the planes (112), (220), and (116). It is known that in this case we can determine L and ε in directions perpendicular to the families of these crystallographic planes [36].

The results of calculations of L and ε for films of solid solutions are systematized in Table 2. As can be seen from the table, the maximum size, which varies from 6.0 to 10.3 nm, has CSR in the direction [116]. With increasing the magnesium content of the precursor, the size first increases, reaching a maximum value at a content of Mg equal to $y = 0.1$, and then begins to decrease monotonically. The size of the CSR behaves in a similar way in the [220] direction, but these dimensions themselves are smaller, varying in the range $L_{(220)}$ = (5.3–6.4) nm. The size of the CSR in the direction [112] increases almost monotonically from (4.6–4.7) nm to (5.2–5.3) nm with an increasing amount of magnesium in the precursor, which was used to obtain the films. However, these values may not be entirely correct due to the overlap of the diffraction peaks (112) and (103), (116) and (303) as already mentioned above. The obtained results indicate different-axial behavior of CSR in the films. The

Table 1
Structural characteristics of $Cu_2Mg_xZn_{1-x}SnS_4$ films.

y	$a_{(220)}$, nm	$a_{(116)}$, nm	$a_{N\text{-}R}$, nm	$c_{(116)}$, nm	$c_{N\text{-}R}$, nm	$c_{(116)}/2a_{(116)}$	$c_{N\text{-}R}/2a_{N\text{-}R}$	$V_{unit\ (116)}$, nm^3	$V_{unit\ (N\text{-}R)}$, nm^3
0	0.54097	0.54443	0.54140	1.08903	1.08214	1.00016	0.99939	0.323	0.317
0.1	0.54043	0.54399	0.54099	1.08794	1.08289	0.99996	1.00084	0.322	0.317
0.2	0.54151	0.54265	0.54246	1.08468	1.08681	0.99943	1.00174	0.319	0.320
0.3	0.54204	0.54399	0.54421	1.08794	1.09289	0.99996	1.00411	0.322	0.324
0.4	0.54297	0.54399	0.54340	1.08794	1.09289	0.99996	1.00560	0.322	0.323
0.5	0.54475	0.54488	0.54728	1.09013	1.09675	1.00034	1.00200	0.324	0.328
Reference (JCPDS # 00–033–0492)		0.54340			0.99889		1.0856		0.321

Table 2
Microstructural characteristics of $Cu_2Mg_xZn_{1-x}SnS_4$ films.

y	$L_{(112)}$, nm	$\varepsilon_{(112)}\cdot10^{-3}$	$L_{(220)}$, nm	$\varepsilon_{(220)}\cdot10^{-3}$	$L_{(116)}$, nm	$\varepsilon_{(116)}\cdot10^{-3}$	$\rho_{L(220)}\cdot10^{-17}$, lin/m^{-2}	$\rho_{\varepsilon(220)}\cdot10^{-16}$, lin/m^{-2}	$\rho_{\varepsilon L(220)}\cdot10^{-17}$, lin/m^{-2}
0	4.7	8.3	5.3	7.2	6.3	6.2	1.07	2.25	1.06
0.1	4.6	8.4	6.4	6.0	10.3	3.7	0.73	1.56	0.73
0.2	4.9	7.8	5.4	7.1	7.9	4.9	1.03	2.19	1.03
0.3	5.0	7.7	5.8	6.7	6.2	6.2	0.89	1.95	0.90
0.4	5.3	7.3	5.3	7.2	6.0	6.4	1.07	2.25	1.06
0.5	5.2	7.4	5.3	7.2	6.1	6.3	1.07	2.25	1.06

values of CSR sizes found in our films correlate well with the values calculated by the authors [49,50].

However, the obtained values in the directions [112] and [116] may not be accurate enough due to the overlap of the diffraction peaks (112)-(103) and (116)-(303), as already mentioned above.

The level of microdeformations in the samples decreases monotonically from $\varepsilon_{(112)} \sim (8.3–8.4)\cdot10^{-3}$ to $\varepsilon_{(112)} \sim (7.3–7.4)\cdot10^{-3}$ for the direction [112] with increasing magnesium content in the precursor. Simultaneously, for the other two directions ([220], [116]) on the curve ($\varepsilon - y$) a minimum is observed at a concentration of magnesium equal to $y = 0.1$. The values of the level of microdeformations found by the reflections from the crystallographic planes (116) and (220) are smaller than for the reflections (112). Thus, both the size of the CSR and the level of microdeformations in the films depend on the crystallographic direction of the material.

As already indicated, the small-angle boundaries of the CSR are formed by dislocations. These dislocations are located in the volume of the block and lead to microdeformations in the material. Therefore, it is possible to estimate the average density of dislocations in $Cu_2Mg_xZn_{1-x}SnS_4$ films by the magnitude of their microdeformations ε and the size of the CSR L.

Calculations of the concentration of dislocations at the boundaries of the CSR ($\rho_{L(220)}$), in their volume ($\rho_{\varepsilon(220)}$), and the total concentration of dislocations ($\rho_{\varepsilon L(220)}$) were carried out using the expressions presented in the methodology. The obtained results are shown in Table 3. In this case, the values of L and ε in the direction [220] were used since the other reflections are a superposition of two closely spaced diffraction lines ([112–103]), ([116–303]).

It was established that the studied films have a pretty high concentration of dislocations (10^{-16}-10^{-17} lin/m^{-2}). Calculations show that the dislocations are concentrated mainly on the boundaries of the CSR. Taking into account this fact, it can be stated that the volume of films is almost free of dislocations. It is shown that with an increase in the magnesium content in the precursor, the concentration of dislocations at the boundaries of CSR ρ_L in the films initially decreases from $1.07\cdot10^{-17}$ lin/m^{-2} ($y = 0$) to $0.73\cdot10^{-17}$ lin/m^{-2} ($y = 0.1$), and then increases to $1.07\cdot10^{-17}$ lin/m^{-2} ($y = 0.5$) (calculations according to relation (7)). The concentration of dislocations in the inside of the CSR ρ_ε behaves similarly, decreasing from $2.25\cdot10^{-16}$ lin/m^{-2} ($y = 0$) to $1.56\cdot10^{-16}$ lin/m^{-2} ($y = 0.1$) and increasing to $2.25\cdot10^{-16}$ lin/m^{-2} ($y = 0.5$) (calculations according to relation (8)). Thus, films obtained from a precursor containing magnesium equal to $y = 0.1$ have the minimum concentration of dislocations. Calculations of the total concentration of dislocations in the samples according to relation (9) give results similar to those obtained using expressions (7) and (8). The general trends in the behavior of the dependence $\rho_{\varepsilon L(220)}$ - y are preserved.

We performed the chemical analysis of $Cu_2Mg_xZn_{1-x}SnS_4$, films obtained from precursors with different magnesium content by the EDX method. The corresponding results are presented in Table 3. The Table 3 also shows the composition of the stoichiometric compound Cu_2ZnSnS_4; composition of the most optimal for the creation of high efficiency SCs; the calculated ratio of the concentrations of the components of the compound to create devices based on them. The results obtained using two different detectors (X-MaxN20, Bruker*) mainly (except for the magnesium content) coincided with the accuracy of the method. Therefore, the type of detector will not be specified in the future, and the table (except for C_{Mg}*) shows the results obtained using the detector X-MaxN20.

It was found that for the sample which did not contain Mg, the values of concentration C_{Cu}: C_{Zn}: C_{Sn}: C_S= 25.15: 11.83: 13.33: 49.5, were close to the atomic concentrations of the stoichiometric compound $Cu_2ZnSnSe_4$ – C_{Cu}: C_{Zn}: C_{Sn}: C_S = 25.0: 12.5: 12.5: 50.0. This indicates that the method of synthesis used by us makes it possible to obtain films with a element's ratio of the compound close to the theoretical one. As can be seen from Table 3, the value of the atomic concentration of Cu, Sn, S elements in $Cu_2Mg_xZn_{1-x}SnS_4$ films depends on the ratio of Mg content to Zn content. However, it should be noted, that this composition varied slightly with the amount of magnesium in the precursor. Only in the case of sulfur, the introduction of magnesium reduced its concentration in the compound.

The results presented in Table 3 also indicate that the Mg content in the films with increasing its concentrations in the precursor increases almost linearly. The value in the film obtained from the precursor with nominal Mg content $y = 0.5$ reaches (5.78–8.51) at%, according to various detectors of different EDX equipment. It is also possible to observe a gradual decrease in the Zn content in the films with an increase in the Mg content, which indicates the successful replacement of Zn ions by Mg ions in the crystal lattice of the samples.

Thus, considering the obtained results, we can say that it was possible to obtain films $Cu_2Mg_xZn_{1-x}SnS_4$, which have a composition close to stoichiometric. It should also be noted that our proposed method allowed to obtain layers of kesterites that have a high level

Table 3
Chemical composition of $Cu_2Mg_xZn_{1-x}SnS_4$ films.

y	EDAX							Stoichiometry		
	C_S, at%	C_{Cu}, at%	C_{Zn}, at%	C_{Sn}, at%	C_{Mg}, at%	C_{Mg^*}, at%	$C_{(Zn+Mg)}$, at%	$C_{Cu}/C_{(Zn+Mg+Sn)}$	$C_{(Zn+Mg)}/C_{Sn}$	$C_{Mg}/C_{(Mg+Zn)}$
0	49.45	25.15	11.83	13.33	0	0	11.83	1.00	0.89	0
0.1	45.32	25.43	11.60	13.73	3.91	3.77	15.51	0.87	1.13	0.25
0.2	46.18	23.88	12.04	12.11	5.77	6.80	17.81	0.80	1.47	0.32
0.3	46.75	26.59	8.40	14.32	3.94	5.64	12.34	1.00	0.86	0.32
0.4	46.80	26.21	7.09	13.93	6.70	7.21	13.79	0.95	0.99	0.49
0.5	48.43	24.93	6.32	14.54	5.78	8.51	12.10	0.94	0.83	0.48
Stoichiometric composition	50.00	25.00	12.5	12.50			12.50			
The optimal composition of effective SC	50.00	22.20	14.6	13.20			14.60			

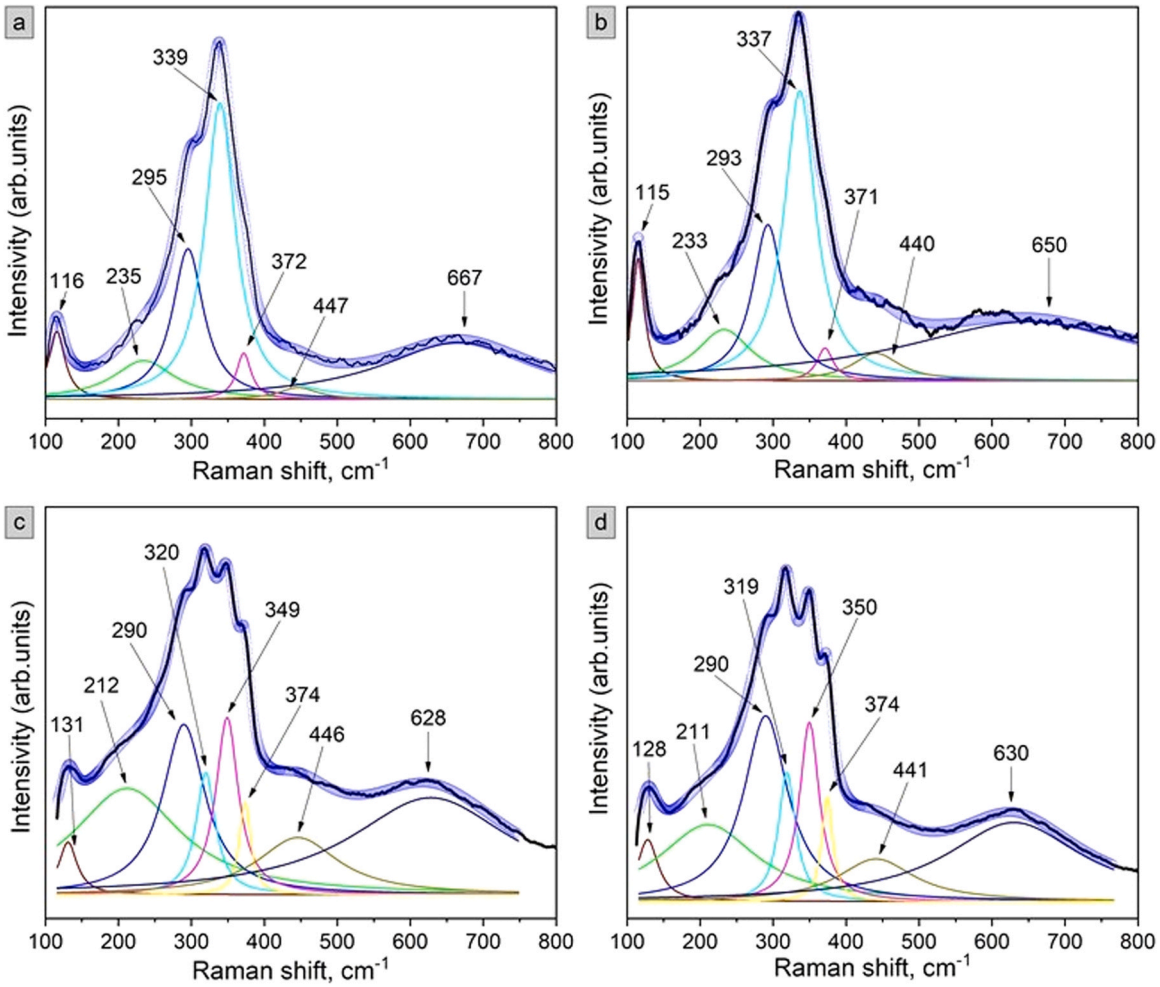

Fig. 4. Raman spectra of films $Cu_2Mg_xZn_{1-x}SnS_4$ obtained from precursors with different nominal Mg content: $y = 0$ (Cu_2ZnSnS_4) (a); $y = 0.2$ (b); $y = 0.3$ (c); $y = 0.5$ (d).

of Zn, which previously was quite problematic, especially in the case of nanoparticles of kesterite compounds [51,52].

It is known that in the compound Cu_2ZnSnS_4 it is possible to find secondary phases of both binary and ternary, such as cubic Cu_xS_y, Zn_xS_y, and Sn_xS_y, tetragonal Cu_xSnS_y and Zn_xSnO_y, etc. [53]. They have crystal lattices close to the kesterite compound, which reflects at angles similar to the angles obtained from the Cu_2ZnSnS_4 compound [54]. This makes it difficult to detect of secondary phases of the material by XRD. Therefore, to accurately identify the single-phase solid solution of $Cu_2Mg_xZn_{1-x}SnS_4$, the studied samples were additionally studied by Raman spectroscopy. The results of these studies, depending on the ratio of Mg content to Zn content in precursors, are shown in Fig. 4. Decomposition of experimental spectra into components was carried out by representing individual peaks by a Lorentzian function, which allowed us to accurately determine their position.

As can be seen from Fig. 4a, the Raman spectrum of the film obtained from the precursor which did not contain magnesium (Cu_2ZnSnS_4), corresponds to the reference. However, in this case these peaks overlap as a result of their large half-widths. The obtained results are in good agreement with those previously reported in [45,47]. It is known [55], that for the bulk compound Cu_2ZnSnS_4, Raman spectra contain three peaks in the frequency range (150–450) cm^{-1}. The most intense peaks correspond to the frequencies (331–339) cm^{-1}. Besides, two less intense peaks also observed at frequencies (287–289) cm^{-1} and (368–373) cm^{-1}. These Raman peaks are usually attributed to the modes of oscillations A (287 cm^{-1}), A (338 cm^{-1}), and E (368 cm^{-1}), associated with the S atom in the kesterite compound [27]. In addition, in some works [56,57] there are also peaks at frequencies of 142 cm^{-1} and (672–676) cm^{-1} associated with E and 2 A modes (phonon repetition of A mode).

Similar peaks at 116, 295, 339, 372, and 667 cm^{-1} are presented in the spectrum of the studied sample Cu_2ZnSnS_4 and can be interpreted as E, A, A, 2 A mode, respectively. Some shift of the peaks from those characteristic of the bulk material may be due to the film nature of the samples and the presence of microdeformations into them. In addition, the decomposition of the Raman spectrum into components reveals low-intensity maxima at frequencies of 235 and 447 cm^{-1}, which we have not interpreted, but most likely they are not associated with traditional secondary phases (Cu_2SnS_3, SnS_2, SnS, ZnS), which occur in the kesterite compound. These peaks are observed in the spectra of the films containing magnesium. No other peaks were observed in the Raman spectra.

As can be seen from Fig. 5, with increasing magnesium content in the precursor and, accordingly, in the films, the peaks in the Raman spectra undergo frequency shift. Thus, the most intense peak corresponding to the vibrational mode A shifts to the red region of the spectrum from the frequency 339 cm^{-1} for $y = 0.0$–319 cm^{-1} for $y = 0.5$. This is clearly seen in Fig. 6a, where the dependence of the frequency of displacement of the main modes of the films of the solid solution $Cu_2Mg_xZn_{1-x}SnS_4$ on the magnesium content in the precursor is shown. It should be noted that the displacement is significantly enhanced in samples obtained from a precursor containing magnesium, where $y > 0.2$.

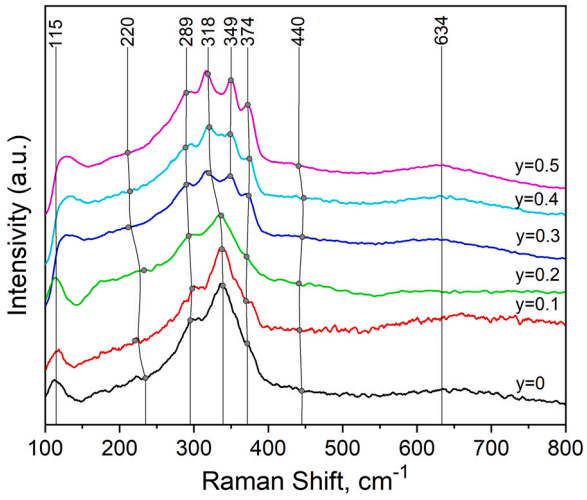

Fig. 5. Raman spectra of $Cu_2Mg_xZn_{1-x}SnS_4$ films with different nominal Mg content.

The peak is associated with another phonon mode A, shifts to the red region from 295 cm^{-1} to 290 cm^{-1}. At the same time, the peak corresponding to the mode E is shifted much less from values of 372 cm^{-1} to values of 374 cm^{-1}. In accordance with the results of X-ray studies, the change in the position of the A peaks can be explained by the change in the distances between atoms in solid solution $Cu_2Mg_xZn_{1-x}SnS_4$ due to the replacement of smaller Zn^{2+} ions with larger Mg^{2+} ions. The red shift in lattice oscillations is usually explained by the lower strength of Mg–S bonds than in Zn–S, due to the larger covalent radius of Mg than in Zn [45]. As was previously reported in [46], a similar shift of the most intense Raman peak at 337 cm^{-1} (Cu_2ZnSnS_4) to the red region to 317 cm^{-1} (Cu_2MgSnS_4) caused by the replacement of zinc ions with magnesium.

The change in the full width at half maximum (FWHM) of the main modes of the solid solution $Cu_2Mg_xZn_{1-x}SnS_4$ depending on the magnesium content in the precursor is shown in Fig. 6b. It is seen that the FWHM value of the most intensive mode (339 cm^{-1} for undoped film) decreases monotonically with increasing magnesium content in the samples. At the same time, the dependence on other modes is more complex. Thus, the FWHM of the mode *E* (372 cm^{-1}) first increases, reaching the maximum value for the film with a nominal magnesium content of $y = 0.1$, and then decreases. The dependence of FWHM for mode A (295 cm^{-1}) has a minimum at the nominal composition of Mg of $y = 0.2$, and with a further increase in this concentration increases. Usually, a decrease in the FWHM of Raman peaks is associated with an improvement in crystal structure. At the same time their broadening is caused with its deterioration [58]. In our case, since the change in the FWHM of the peaks of different modes is multidirectional, it is difficult to judge the nature of the change in the structural quality of films.

It should be noted that the shape of the spectra of samples deposited from a nominal magnesium content $y > 0.3$ varies significantly compared to samples with a lower nominal magnesium content and an additional peak appears in the spectrum at a frequency (349–350) cm^{-1}. Its position is close to the peaks observed in the Raman spectra of compounds such as ZnS (352 cm^{-1}) and Cu_2SnS_3 (352–356) cm^{-1}. Taking into account the fact that Mg in the lattice of the material replaces Zn, which becomes excess, in our opinion, we should rather expect the formation of the compound ZnS. However, at lower Mg values we were able to obtain films of solid solutions of $Cu_2Mg_xZn_{1-x}SnS_4$ of different compositions with the ability to control the content of Mg and Zn, which improves the electrophysical and optical characteristics of the material.

The study of the optical spectra of film semiconductor materials makes it possible to determine one of their most important characteristics, namely, the band gap E_g. As previously shown by us one accurate method of determining this parameter is to measure the exciton absorption or reflection spectra [59,60]. In the case of thin films (about 1 μm) both optical methods can be used, and for thicker films, only measurements of exciton reflection spectra can be used. This makes it possible to determine the energy position of the free excitons and to determine the value of E_g on the basis of the obtained results since this value is equal to the energy of the free exciton plus the energy of its binding. This approach requires measurements at low temperatures and the presence of high optical quality of the studied film materials. The fact is that the presence of different types of defects, both intrinsic and impurity, can lead to a significant broadening of the exciton lines of absorption or reflection, which can make it difficult to determine the energy position of their maximum. Therefore, the literature uses a common method for determining the band gap by approximating the absorption edge using the Tauc's relation, which for direct allowed band-band optical transitions is as follows:

$$(\alpha h\nu)^2 = A(h\nu\text{-}E_g), \tag{10}$$

where *A* – a constant that reflects the slope of the approximation curve in the region of its linearity, $h\nu$ – the energy of light, E_g – the band gap energy.

The value of E_g is determined based on the dependence $(\alpha h\nu)^2$ on energy ($h\nu$) [59,60]. Approximation of a straight line to its

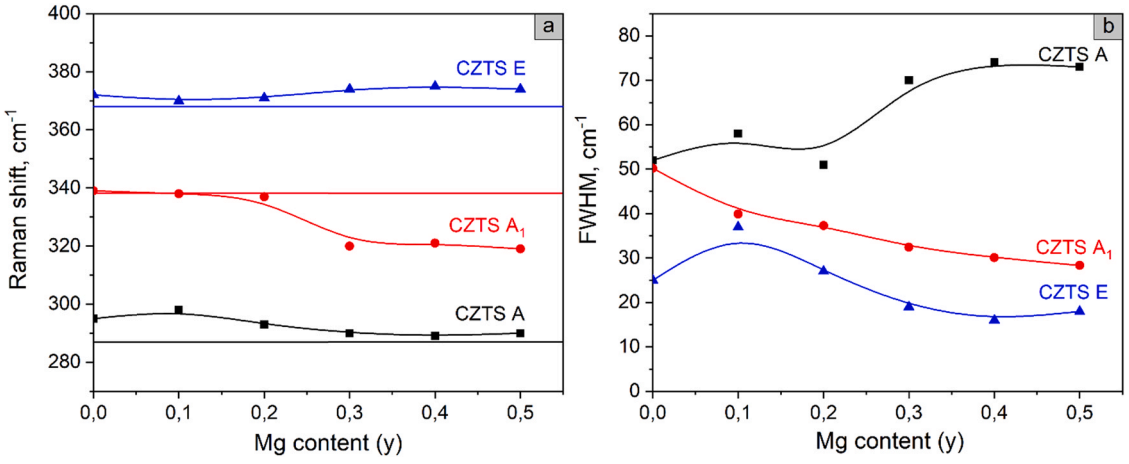

Fig. 6. Dependence of the frequency of displacement of the main modes of $Cu_2Mg_xZn_{1-x}SnS_4$ films (a) and the half-width of these peaks (b) on the magnesium content in the precursor. Solid straight lines – are reference data.

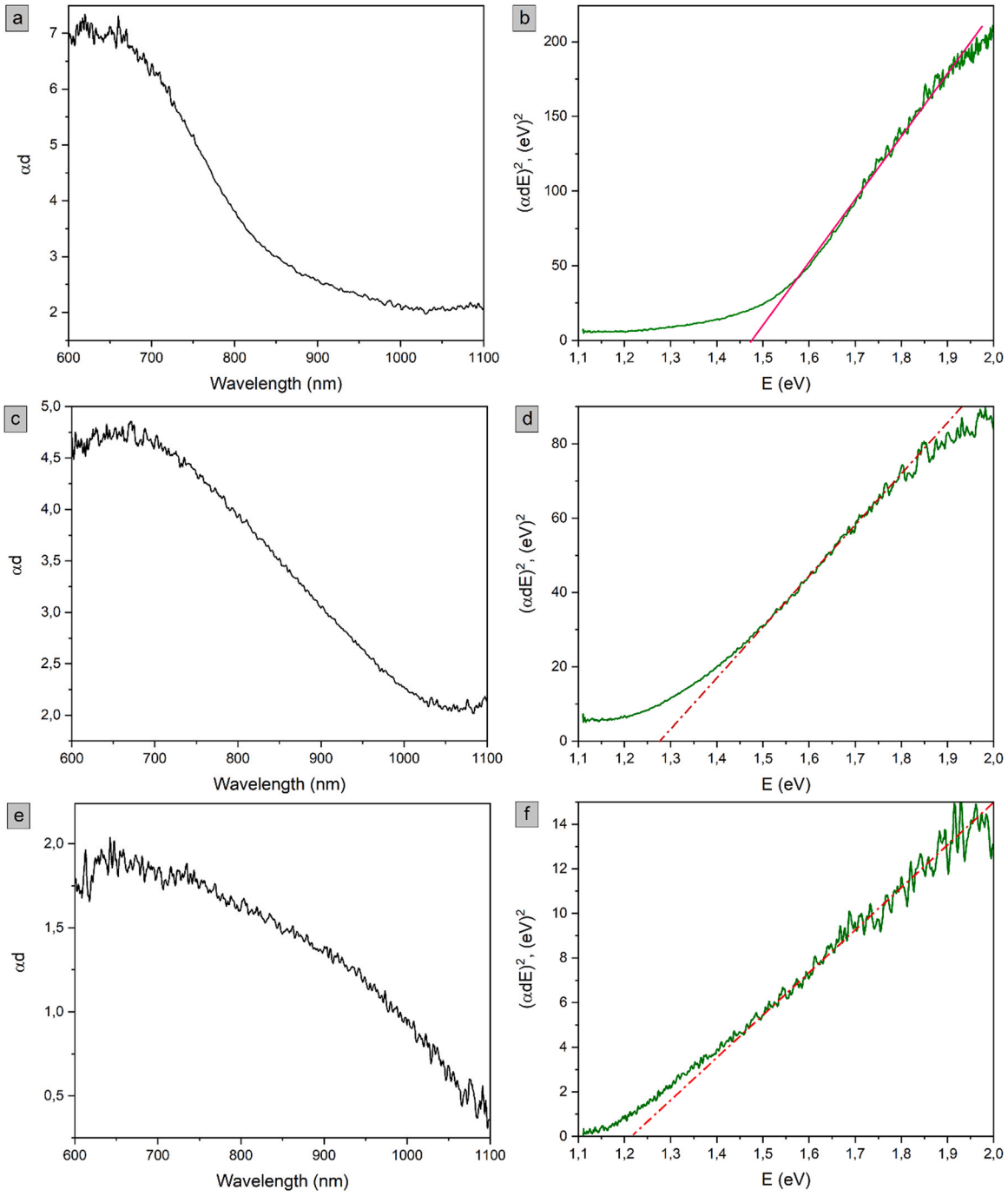

Fig. 7. The optical density spectrum at room temperature and determination of the band gap energy by approximating the absorption edge of $Cu_2Mg_xZn_{1-x}SnS_4$, where $y = 0$ (a, b); $y = 0.1$ (c, d), $y = 0.5$ (e, f).

intersection with the energy axis determines the value of E_g. The resulting value is called the optical band gap. However, this value is somewhat underestimated compared to the value of E_g obtained from the measurement of exciton absorption or reflection spectra, where the energy is determined by the position of the exciton absorption maximum. At the same time, in the case of approximation of the absorption edge by the Tauc's method, the band gap energy is determined by the intersection of the linear dependence $(\alpha h\nu)^2$ on the energy with the energy axis, i.e. it corresponds to the edge absorption at much lower (in several orders) absorption coefficient values. It should be noted that the tightened shape of the long-wavelength absorption edge is determined by the absorption as a result of the manifestation of electron (exciton)-phonon interaction, and optical transitions involving energy levels of various defects.

Theoretical calculations show that the value of the band gap for Cu_2ZnSnS_4 depends on the type of crystal lattice. Thus, in the case of kesterites, this value in different works is 1.64 eV and 1.56 eV, while for stanites the band gap value is lower, 1.33 and 1.42 eV [61,62]. It has also been found theoretically that the band gap of Cu_2ZnSnS_4 kesterites strongly depends on the magnitude of the Sn-S chemical bond [63]. If this value is reduced by 5%, the value of the band gap increases to 1.80 eV. At the same time, stretching of such a chemical bond by 4% leads to a decrease in the value of E_g to 1.15 eV. In nanocrystals and films, there is always some deformation of the crystal lattice, which can lead to changes in the length of the chemical bond

Sn-S. Therefore, in nanocrystals, the value of E_g may depend on the technological conditions for obtaining kesterite material. This may be the reason for the variety of values of E_g given in the literature for kesterite semiconductors.

Fig. 7a shows the spectral dependence of the product of the absorption coefficient and the thickness of nanostructured Cu_2ZnSnS_4 films obtained at room temperature i.e. the optical density of the studied films. It is seen that the absorption of the sample begins to increase at wavelengths less than 1000 nm. The absorption edge is quite steep, which indicates a sufficiently good crystalline and optical quality of the studied films. The optical density of the film in the short-wavelength part of the spectrum changes almost linearly with decreasing wavelength. At a certain value of energy, the optical density is almost saturated as a result of the fact that there is a weak transmission, which can't be experimentally recorded.

Since the method of determining the band gap of semiconductor materials by approximating the long-wavelength edge of fundamental absorption is widely used in the literature, we also performed a similar approximation for the studied Cu_2ZnSnS_4 films using relation (4). The results of the approximation are presented in Fig. 7b indicates that the value of E_g for Cu_2ZnSnS_4 is 1.47 eV, which agrees well with both theoretical and experimental values available in the literature. This indicates that the compound has a kesterite structure.

Fig. 7c,d shows the optical density spectrum and approximates the absorption edge obtained for thin layers obtained from a precursor with a $y = 0.1$. The approximation of the obtained spectrum is similar to that performed for undoped samples. The results show that the value of E_g for these films decreases slightly and is 1.28 eV. A decrease in E_g may be associated with the formation of solid solutions. The reason may also be the deformation of Cu_2ZnSnS_4 nanocrystals when Mg impurities are introduced, which can cause changes in the parameters of chemical bonds. An increase in the impurity concentration to $y = 0.5$, as shown by the results presented in Fig. 7e,f, leads to a further decrease in the value of E_g to 1.22 eV. The low-temperature photoluminescence spectrum of undoped Cu_2ZnSnS_4 films is presented in Fig. 8. As can be seen from Fig. 8, the photoluminescence spectrum of Cu_2ZnSnS_4 films at $T = -196$ ºC has the form of a broad band with a maximum of 795 nm (1.56 eV).

The obtained value of band gap energy is slightly higher in comparison with the value of the band gap (1.47 eV), obtained on the basis of the results of the approximation of the absorption edge by the Tauc's method. This is due to the difference in the nature of electronic mechanisms that determine the processes of photoluminescence and absorption processes in the studied films.

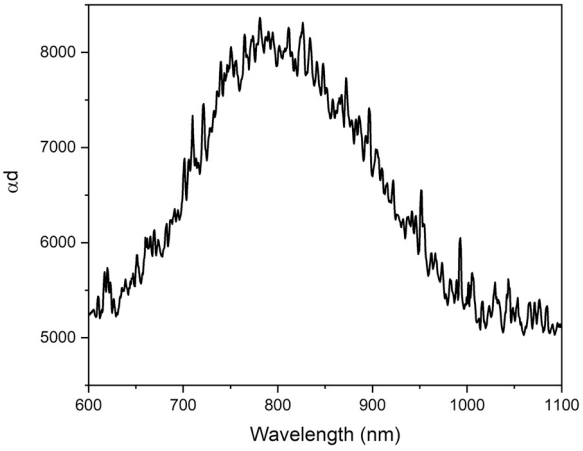

Fig. 8. Photoluminescence spectrum for undoped Cu_2ZnSnS_4 films at T=-196ºC.

4. Conclusions

In this work, $Cu_2Mg_xZn_{1-x}SnS_4$ films with different Mg content were obtained using the spray pyrolysis method. Here, molecular solutions with a molar ratio of Mg to Zn concentration in the interval $0 \le y \le 0.5$ were used. The content of Mg in the films increases almost linearly from 0 to 5.78 at% with increase it's in the precursor. In this case, zinc is replaced by magnesium in the crystal lattice. It was shown that the chemical composition of the obtained samples was close to stoichiometric ratio. X-ray diffractometric analysis and Raman studies show that the obtained films have a pure kesterite phase at $y < 0.3$. An increase in the value of y led to the appearance of traces of the ZnS compound in the films. The introduction of Mg leads to an increase in the lattice constants of the material from $a_{N\text{-}R}$ = 0.54140 nm and $c_{N\text{-}R}$ = 1.08214 nm at $y = 0$ to $a_{N\text{-}R}$ = 0.54728 and $c_{N\text{-}R}$ = 1.09675 nm for $y = 0$ and $y = 0.5$, respectively.

It was shown that the size of the CSR for different crystallographic directions varies from 4.6 to 10.3 nm and depends on the concentration of magnesium. This indicates that CSRs have a non-equiaxial form. Based on the results of measuring the size of the CSR and the level of microdeformations for the studied films, the density of dislocations was calculated, which varied in the interval $\rho_{\varepsilon L(220)} = (0.73\text{–}1.06)\cdot 10^{-17}$ lin/m^{-2}. It should be noted that the films obtained at $y = 0.1$ have the minimum total concentration of dislocations ($\rho_{\varepsilon L(220)} = 0.73\cdot 10^{-17}$ lin/m^{-2}). It was also found that replacing zinc with magnesium increases the structural quality of the solid solution at $y < 0.3$. Therefore, one can expect a decrease in the rate of recombination of photogenerated carriers in photosensitive devices developed on the basis of such films.

The study of the optical spectra of the films made it possible to determine the value of the band gap energy in the obtained samples. It was found that for the undoped material this value correspond to 1.47 eV, and for the samples doped with Mg, it decreases from 1.28 eV ($y = 0.1$) to 1.22 eV ($y = 0.5$). Thus, the obtained results show that the introduction of magnesium into the Cu_2ZnSnS_4 compound has a similar effect to selenium, bringing the value E_g closer to the Shockley-Queiser optimum characteristic for the most efficient SCs. We assume that the films obtained from a precursor with $0.1 \le y \le 0.2$, which have the best structural quality, can be considered as promising absorbing layers for third-generation SCs.

CRediT authorship contribution statement

Maksym Yermakov: Conceptualization, Investigation, Data curation. **Roman Pshenychnyi:** Investigation, Data curation. **Anatoliy Opanasyuk:** Conceptualization, Writing – original draft preparation. **Yuriy Gnatenko:** Methodology, Writing – reviewing and editing. **Oleksii Klymov:** Visualization, Investigation. **María del Carmen Martínez-Tomás:** Validation. **Vicente Muñoz-Sanjosé:** Supervision.

Data availability

Data will be made available on request.

Declaration of Competing Interest

The authors declare that they have no known competing financial interests or personal relationships that could have appeared to influence the work reported in this paper.

Acknowledgments

This work was supported by the Science for Peace and Security Programme for the NATO [grant number G5916].

References

[1] S. Temgoua, R. Bodeux, F. Mollica, N. Naghavi, Comparative study of $Cu_2ZnSnSe_4$ solar cells growth on transparent conductive oxides and molybdenum substrates, Sol. Energy 194 (2019) 121–127, https://doi.org/10.1016/j.solener.2019.10.050

[2] L. Et-taya, T. Ouslimane, A. Benami, Numerical analysis of earth-abundant $Cu_2ZnSn(S_xSe_{1-x})_4$ solar cells based on spectroscopic ellipsometry results by using SCAPS-1D, Sol. Energy 201 (2020) 827–835, https://doi.org/10.1016/j.solener.2020.03.070

[3] F. Liu, S. Shen, F. Zhou, N. Song, X. Wen, J.A. Stride, K. Sun, C. Yan, X. Hao, Kesterite Cu_2ZnSnS_4 thin film solar cells by a facile DMF-based solution coating process, J. Mater. Chem. C. Mater. 3 (2015) 10783–10792, https://doi.org/10.1039/c5tc01750e

[4] C. Yan, J. Huang, K. Sun, S. Johnston, Y. Zhang, H. Sun, A. Pu, M. He, F. Liu, K. Eder, L. Yang, J.M. Cairney, N.J. Ekins-Daukes, Z. Hameiri, J.A. Stride, S. Chen, M.A. Green, X. Hao, Cu_2ZnSnS_4 solar cells with over 10% power conversion efficiency enabled by heterojunction heat treatment, Nat. Energy 3 (2018) 764–772, https://doi.org/10.1038/s41560-018-0206-0

[5] R. Fonoll-Rubio, J. Andrade-Arvizu, J. Blanco-Portals, I. Becerril-Romero, M. Guc, E. Saucedo, F. Peiró, L. Calvo-Barrio, M. Ritzer, C.S. Schnohr, M. Placidi, S. Estradé, V. Izquierdo-Roca, A. Pérez-Rodríguez, Insights into interface and bulk defects in a high efficiency kesterite-based device, Energy Environ. Sci. 14 (2021) 507–523, https://doi.org/10.1039/d0ee02004d

[6] N. Mufti, T. Amrillah, A. Taufiq, Sunaryono, Aripriharta, M. Diantoro, Zulhadjri, H. Nur, Review of CIGS-based solar cells manufacturing by structural engineering, Sol. Energy 207 (2020) 1146–1157, https://doi.org/10.1016/j.solener.2020.07.065

[7] C. Yan, K. Sun, F. Liu, J. Huang, F. Zhou, X. Hao, Boost Voc of pure sulfide kesterite solar cell via a double CZTS layer stacks, Sol. Energy Mater. Sol. Cells 160 (2017) 7–11, https://doi.org/10.1016/j.solmat.2016.09.027

[8] L. Sravani, S. Routray, M. Courel, K.P. Pradhan, Loss mechanisms in CZTS and CZTSe Kesterite thin-film solar cells: understanding the complexity of defect density, Sol. Energy 227 (2021) 56–66, https://doi.org/10.1016/j.solener.2021.08.052

[9] M. Kumar, A. Dubey, N. Adhikari, S. Venkatesan, Q. Qiao, Strategic review of secondary phases, defects and defect-complexes in kesterite CZTS-Se solar cells, Energy Environ. Sci. 8 (2015) 3134–3159, https://doi.org/10.1039/c5ee02153g

[10] J.K. Larsen, J.J.S. Scragg, N. Ross, C. Platzer-Björkman, Band tails and Cu-Zn disorder in Cu2ZnSnS4Solar cells, ACS Appl. Energy Mater. 3 (2020) 7520–7526, https://doi.org/10.1021/acsaem.0c00926

[11] J.J.S. Scragg, J.K. Larsen, M. Kumar, C. Persson, J. Sendler, S. Siebentritt, C. Platzer Björkman, Cu-Zn disorder and band gap fluctuations in Cu2ZnSn(S,Se)4: Theoretical and experimental investigations, Phys. Status Solidi B Basic Res 253 (2016) 247–254, https://doi.org/10.1002/pssb.201552530

[12] W. Li, X. Liu, H. Cui, S. Huang, X. Hao, The role of Ag in $(Ag,Cu)_2ZnSnS_4$ thin film for solar cell application, J. Alloy. Compd. 625 (2015) 277–283, https://doi.org/10.1016/j.jallcom.2014.11.136

[13] L. Meng, B. Yao, Y. Li, Z. Ding, Z. Xiao, K. Liu, G. Wang, Significantly enhancing back contact adhesion and improving stability of $Cu_2(Zn,Cd)Sn(S,Se)_4$ solar cell by a rational carbon doping strategy, J. Alloy. Compd. 710 (2017) 403–408, https://doi.org/10.1016/j.jallcom.2017.03.281

[14] R. Chen, C. Persson, Electronic and optical properties of Cu_2XSnS_4 (X = Be, Mg, Ca, Mn, Fe, and Ni) and the impact of native defect pairs, J. Appl. Phys. 121 (2017) 203104, https://doi.org/10.1063/1.4984115

[15] J. Li, Y. Huang, J. Huang, G. Liang, Y. Zhang, G. Rey, F. Guo, Z. Su, H. Zhu, L. Cai, K. Sun, Y. Sun, F. Liu, S. Chen, X. Hao, Y. Mai, M.A. Green, Defect Control for 12.5% Efficiency $Cu_2ZnSnSe_4$ Kesterite Thin-Film Solar Cells by Engineering of Local Chemical Environment, Adv. Mater. 32 (2020) 2005268, https://doi.org/10.1002/adma.202005268

[16] S. Ma, H. Li, J. Hong, H. Wang, X. Lu, Y. Chen, L. Sun, F. Yue, J.W. Tomm, J. Chu, S. Chen, Origin of Band-Tail and Deep-Donor States in Cu_2ZnSnS_4 Solar Cells and Their Suppression through Sn-Poor Composition, J. Phys. Chem. Lett. 10 (2019) 7929–7936, https://doi.org/10.1021/acs.jpclett.9b03227

[17] S. Giraldo, M. Neuschitzer, T. Thersleff, S. López-Marino, Y. Sánchez, H. Xie, M. Colina, M. Placidi, P. Pistor, V. Izquierdo-Roca, K. Leifer, A. Pérez-Rodríguez, E. Saucedo, Large Efficiency Improvement in $Cu_2ZnSnSe_4$ Solar Cells by Introducing a Superficial Ge Nanolayer, Adv. Energy Mater. 5 (2015) 1501070, https://doi.org/10.1002/aenm.201501070

[18] S. Giraldo, E. Saucedo, M. Neuschitzer, F. Oliva, M. Placidi, X. Alcobé, V. Izquierdo-Roca, S. Kim, H. Tampo, H. Shibata, A. Pérez-Rodríguez, P. Pistor, How small amounts of Ge modify the formation pathways and crystallization of kesterites, Energy Environ. Sci. 11 (2018) 582–593, https://doi.org/10.1039/c7ee02318a

[19] S.A. Vanalakar, P.S. Patil, J.H. Kim, Recent advances in synthesis of Cu_2FeSnS_4 materials for solar cell applications: a review, Sol. Energy Mater. Sol. Cells 182 (2018) 204–219, https://doi.org/10.1016/j.solmat.2018.03.021

[20] K. Rudisch, W.F. Espinosa-García, J.M. Osorio-Guillén, C.M. Araujo, C. Platzer-Björkman, J.J.S. Scragg, Structural and electronic properties of Cu_2MnSnS_4 from experiment and first-principles calculations, Phys. Status Solidi (b) 256 (2019) 1800743, https://doi.org/10.1002/pssb.201800743

[21] S. Hadke, S. Levcenko, G. Sai Gautam, C.J. Hages, J.A. Márquez, V. Izquierdo-Roca, E.A. Carter, T. Unold, L.H. Wong, Suppressed deep traps and bandgap fluctuations in Cu_2CdSnS_4 solar cells with ≈8% efficiency, Adv. Energy Mater. 9 (2019) 1902509, https://doi.org/10.1002/aenm.201902509

[22] D. Friedrich, S. Greil, T. Block, L. Heletta, R. Pöttgen, A. Pfitzner, Synthesis and Characterization of Ag2MnSnS4, a New Diamond-like Semiconductor, Z. Anorg. Allg. Chem. 644 (2018) 1707–1714, https://doi.org/10.1002/zaac.201800142

[23] F.Z. Nainaa, N. Bekkioui, A. Abbassi, H. Ez-Zahraouy, First principle study of structural, electronic optical and electric properties of Ag2MnSnS4, Comput. Condens. Matter 22 (2020) e00443, https://doi.org/10.1016/j.cocom.2019.e00443

[24] F.Z. Nainaa, N. Bekkioui, A. Abbassi, H. Ez-Zahraouy, First principle study of structural, electronic, optical and electric properties of Ag2ZnGeX4(S, Se), Comput. Condens. Matter 19 (2019) e00364, https://doi.org/10.1016/j.cocom.2019.e00364

[25] D. Sun, Y. Ding, L. Kong, Y. Zhang, X. Guo, L. Wei, L. Zhang, L. Zhang, First-principles Study on Mg Doping in Cu_2ZnSnS_4, J. Inorg. Mater. 35 (2020) 1290–1294, https://doi.org/10.15541/jim20200019

[26] Y. Zhang, D. Jiang, Y. Sui, Y. Wu, Z. Wang, L. Yang, F. Wang, S. Lv, B. Yao, Synthesis and investigation of environmental protection and earth-abundant kesterite $Cu_2MgxZn_{1-x}Sn(S,Se)_4$ thin films for solar cells, Ceram. Int 44 (2018) 15249–15255, https://doi.org/10.1016/j.ceramint.2018.05.167

[27] Y. Sui, Y. Zhang, D. Jiang, W. He, Z. Wang, F. Wang, B. Yao, L. Yang, Investigation of optimum mg doping content and annealing parameters of $Cu_2Mg_xZn_{1-x}SnS_4$ thin films for solar cells, Nanomaterials 9 (2019) 955, https://doi.org/10.3390/nano9070955

[28] F.Z. Nainaa, N. Bekkioui, A. Abbassi, H. Ez-Zahraouy, First principle study of structural, electronic optical and electric properties of Ag2MnSnS4, Comput. Condens. Matter 22 (2020) e00443, https://doi.org/10.1016/j.cocom.2019.e00443

[29] M. Wei, Q. Du, R. Wang, G. Jiang, W. Liu, C. Zhu, Synthesis of new earth-abundant kesterite Cu_2MgSnS_4 nanoparticles by hot-injection method, Chem. Lett. 43 (2014) 1149–1151, https://doi.org/10.1246/cl.140208

[30] S. Kakherskyi, R. Pshenychnyi, O. Dobrozhan, J. Vaziev, A. Opanasyuk, Y. Gnatenko, Effect of Different Selenium Precursors on Structural Characteristics and Chemical Composition of $Cu_2ZnSnSe_4$ Nanocrystals, Acta Phys. Pol. A 141 (2022) 487–499, https://doi.org/10.12693/APhysPolA.141.487

[31] S.I. Kakherskyi, O.A. Dobrozhan, R.M. Pshenychnyi, S.I. Vorobiov, Ye.O. Havryliuk, V. Komanicky, S.V. Plotnikov, A.S. Opanasyuk, Influence of Low-Temperature Annealing on the Structure and Chemical Composition of Cu_2ZnSnS_4 Films Deposed on Flexible Polyimide Substrates, Mater. Sci. 57 (2022) 572–581, https://doi.org/10.1007/s11003-022-00580-3

[32] S. Kakherskyi, O. Dobrozhan, A. Opanasyuk, R. Pshenychnyi, Y. Gnatenko, Optimization of Synthesis Conditions of $Cu_2ZnSn(Se_xS_{1-x})_4$ Nanocrystals for Use in Flexible Electronic Devices, in: 2021 IEEE International Conference on Information and Telecommunication Technologies and Radio Electronics (UkrMiCo), IEEE, 2021: pp. 283–288. https://doi.org/10.1109/UkrMiCo52950.2021.9716633.

[33] A.A. Akl, I.M. el Radaf, A.S. Hassanien, An extensive comparative study for microstructural properties and crystal imperfections of Novel sprayed Cu3SbSe3 Nanoparticle-thin films of different thicknesses, Opt. (Stuttg.) 227 (2021) 165837, https://doi.org/10.1016/j.ijleo.2020.165837

[34] O. Dobrozhan, M. Baláž, S. Vorobiov, P. Baláž, A. Opanasyuk, Morphological, structural, optical properties and chemical composition of flexible Cu_2ZnSnS_2 thin films obtained by ink-jet printing of polyol-mediated nanocrystals, J. Alloy. Compd. 842 (2020) 155883, https://doi.org/10.1016/j.jallcom.2020.155883

[35] A.A. Akl, S.A. Mahmoud, S.M. AL-Shomar, A.S. Hassanien, Improving microstructural properties and minimizing crystal imperfections of nanocrystalline Cu2O thin films of different solution molarities for solar cell applications, Mater. Sci. Semicond. Process 74 (2018) 183–192, https://doi.org/10.1016/j.mssp.2017.10.007

[36] D. Kurbatov, A. Opanasyuk, S.M. Duvanov, A.G. Balogh, H. Khlyap, Growth kinetics and stoichiometry of ZnS films obtained by close-spaced vacuum sublimation technique, Solid State Sci. 13 (2011) 1068–1071, https://doi.org/10.1016/j.solidstatesciences.2011.01.017

[37] S.D. Yadav, M. El-Tahawy, S. Kalácska, M. Dománková, D.C. Yubero, C. Poletti, Characterizing dislocation configurations and their evolution during creep of a new 12% Cr steel, Mater. Charact. 134 (2017) 387–397, https://doi.org/10.1016/j.matchar.2017.11.017

[38] A.A. Akl, I.M. el Radaf, A.S. Hassanien, Intensive comparative study using X-Ray diffraction for investigating microstructural parameters and crystal defects of the novel nanostructural ZnGa2S4 thin films, Superlattices Micro 143 (2020) 106544, https://doi.org/10.1016/j.spmi.2020.106544

[39] V. Kosyak, Y. Znamenshchykov, A. Čerškus, Y.P. Gnatenko, L. Grase, J. Vecstaudza, A. Medvids, A. Opanasyuk, G. Mezinskis, Composition dependence of structural and optical properties of $Cd_{1-x}Zn_xTe$ thick films obtained by the close-spaced sublimation, J. Alloy. Compd. 682 (2016) 543–551, https://doi.org/10.1016/j.jallcom.2016.05.065

[40] A. Voznyi, V. Kosyak, P. Onufrijevs, L. Grase, J. Vecstaudža, A. Opanasyuk, A. Medvid, Laser-induced SnS_2-SnS phase transition and surface modification in SnS_2 thin films, J. Alloy. Compd. 688 (2016) 130–139, https://doi.org/10.1016/j.jallcom.2016.07.103

[41] R. v Digraskar, S.M. Mali, S.B. Tayade, A. v Ghule, B.R. Sathe, Overall noble metal free Ni and Fe doped Cu_2ZnSnS_4 (CZTS) bifunctional electrocatalytic systems for enhanced water splitting reactions, Int J. Hydrog. Energy 44 (2019) 8144–8155, https://doi.org/10.1016/j.ijhydene.2019.02.054

[42] Y. Wang, R. Hao, J. Guo, X. Li, S. Fang, H. Liu, S. Sun, Effect of Mg doping on Cu_2ZnSnS_4 solar cells prepared by DMF-based solution method, Opt. Mater. (Amst.) 117 (2021) 111211, https://doi.org/10.1016/j.optmat.2021.111211

[43] J. Ge, J. Chu, J. Jiang, Y. Yan, P. Yang, Characteristics of in-substituted CZTS thin film and bifacial solar cell, ACS Appl. Mater. Interfaces 6 (2014) 21118–21130, https://doi.org/10.1021/am505980n
[44] P. Prabeesh, I. Packia Selvam, S.N. Potty, Structural properties of czts thin films on glass and mo coated glass substrates: A rietveld refinement study, Appl. Phys. A Mater. Sci. Process 124 (2018) 225, https://doi.org/10.1007/s00339-018-1649-7
[45] Y. Wang, Y. Yang, C. Zhu, H. Luan, R. Liu, L. Wang, C. Zhao, X. Lv, Boosting the electrical properties of $Cu_2ZnSn(S,Se)_4$ solar cells via low amounts of Mg substituting Zn, ACS Appl. Energy Mater. 3 (2020) 11177–11182, https://doi.org/10.1021/acsaem.0c02121
[46] G.L. Agawane, S.A. Vanalakar, A.S. Kamble, A.V. Moholkar, J.H. Kim, Fabrication of $Cu_2(Zn_xMg_{1-x})SnS_4$ thin films by pulsed laser deposition technique for solar cell applications, Mater. Sci. Semicond. Process 76 (2018) 50–54, https://doi.org/10.1016/j.mssp.2017.12.010
[47] S. Lie, S.W. Leow, D.M. Bishop, M. Guc, V. Izquierdo-Roca, O. Gunawan, L.H. Wong, Improving Carrier-Transport Properties of CZTS by Mg Incorporation with Spray Pyrolysis, ACS Appl. Mater. Interfaces 11 (2019) 25824–25832, https://doi.org/10.1021/acsami.9b05244
[48] T. Ungár, G. Tichy, J. Gubicza, R.J. Hellmig, Correlation between subgrains and coherently scattering domains, Powder Diffr. 20 (2005) 366–375, https://doi.org/10.1154/1.2135313
[49] M.A. Majeed Khan, S. Kumar, M. Alhoshan, A.S. al Dwayyan, Spray pyrolysed Cu_2ZnSnS_4 absorbing layer: A potential candidate for photovoltaic applications, Opt. Laser Technol. 49 (2013) 196–201, https://doi.org/10.1016/j.optlastec.2012.12.012
[50] M. Souli, R. Engazou, L. Ajili, N. Kamoun-Turki, Physical properties evolution of sprayed Cu_2ZnSnS_4 thin films with growth parameters and vacuum annealing, Superlattices Micro 147 (2020) 106711, https://doi.org/10.1016/j.spmi.2020.106711
[51] J. Tao, L. Chen, H. Cao, C. Zhang, J. Liu, Y. Zhang, L. Huang, J. Jiang, P. Yang, J. Chu, Co-electrodeposited Cu_2ZnSnS_4 thin-film solar cells with over 7% efficiency fabricated via fine-tuning of the Zn content in absorber layers, J. Mater. Chem. A Mater. 4 (2016) 3798–3805, https://doi.org/10.1039/c5ta09636g
[52] M. Paris, L. Choubrac, A. Lafond, C. Guillot-Deudon, S. Jobic, Solid-state NMR and Raman spectroscopy to address the local structure of defects and the tricky issue of the Cu/Zn disorder in Cu-poor, Zn-rich CZTS materials, Inorg. Chem. 53 (2014) 8646–8653, https://doi.org/10.1021/ic5012346
[53] M. Kumar, A. Dubey, N. Adhikari, S. Venkatesan, Q. Qiao, Strategic review of secondary phases, defects and defect-complexes in kesterite CZTS-Se solar cells, Energy Environ. Sci. 8 (2015) 3134–3159, https://doi.org/10.1039/c5ee02153g
[54] J.M.R. Tan, Y.H. Lee, S. Pedireddy, T. Baikie, X.Y. Ling, L.H. Wong, Understanding the synthetic pathway of a single-phase quarternary semiconductor using surface-enhanced Raman scattering: A case of wurtzite Cu_2ZnSnS_4 nanoparticles, J. Am. Chem. Soc. 136 (2014) 6684–6692, https://doi.org/10.1021/ja501786s
[55] Z. Tong, C. Yan, Z. Su, F. Zeng, J. Yang, Y. Li, L. Jiang, Y. Lai, F. Liu, Effects of potassium doping on solution processed kesterite Cu_2ZnSnS_4 thin film solar cells, Appl. Phys. Lett. 105 (2014) 223903, https://doi.org/10.1063/1.4903500
[56] M. Dimitrievska, A. Fairbrother, X. Fontané, T. Jawhari, V. Izquierdo-Roca, E. Saucedo, A. Pérez-Rodríguez, Multiwavelength excitation Raman scattering study of polycrystalline kesterite Cu_2ZnSnS_4 thin films, Appl. Phys. Lett. 104 (2014) 021901, https://doi.org/10.1063/1.4861593
[57] D. Dumcenco, Y.-S. Huang, The vibrational properties study of kesterite Cu_2ZnSnS_4 single crystals by using polarization dependent Raman spectroscopy, Opt. Mater. (Amst.) 35 (2013) 419–425, https://doi.org/10.1016/j.optmat.2012.09.031
[58] S.P. Kandare, S.S. Dahiwale, S.D. Dhole, M.N. Rao, R. Rao, Order-disorder transition in Nano-Cu_2ZnSnS_4: a Raman spectroscopic study, Mater. Sci. Semicond. Process 102 (2019) 104594, https://doi.org/10.1016/j.mssp.2019.104594
[59] Y.P. Gnatenko, P.M. Bukivskij, M.S. Furier, A.P. Bukivskii, A.S. Opanasyuk, Temperature dependence of the band gap of high optical quality CdS:Dy thin films based on exciton spectra, Mater. Res Express 5 (2018) 125902, https://doi.org/10.1088/2053-1591/aae298
[60] Y.P. Gnatenko, P.M. Bukivskij, S. Opanasyuk, D.I. Kurbatov, M.M. Kolesnyk, V. v. Kosyak, H. Khlyap, Low-temperature photoluminescence of II-VI films obtained by close-spaced vacuum sublimation, J. Lumin 132 (2012) 2885–2888, https://doi.org/10.1016/j.jlumin.2012.06.003
[61] V. Depredurand, Y. Aida, J. Larsen, T. Eisenbarth, A. Majerus, S. Siebentritt, Surface treatment of CIS solar cells grown under Cu-excess, in: 2011 37th IEEE Photovoltaic Specialists Conference, IEEE, 2011: pp. 000337–000342. https://doi.org/10.1109/PVSC.2011.6185953.
[62] A. Redinger, J. Sendler, R. Djemour, T.P. Weiss, G. Rey, P.J. Dale, S. Siebentritt, Different bandgaps in $Cu_2ZnSnSe_2$: A high temperature coevaporation study, IEEE J. Photo 5 (2015) 641–648, https://doi.org/10.1109/JPHOTOV.2014.2377561
[63] C.J. Tong, H.J. Edwards, T.D.C. Hobson, K. Durose, V.R. Dhanak, J.D. Major, K.P. McKenna, Density functional theory and experimental determination of band gaps and lattice parameters in kesterite $Cu_2ZnSn(S_xSe_{1-x})_4$, J. Phys. Chem. Lett. 11 (2020) 10463–10468, https://doi.org/10.1021/acs.jpclett.0c03205